IRAQI JOURNAL OF APPLIED PHYSICS
Vol. 16, No. 3, July-September 2020, pp. 13-20

Effects of Operation Parameters on Structures and Surface Morphology of Tin Dioxide Nanostructures Prepared by DC Reactive Sputtering

Fuad T. Ibrahim

Department of Physics, College of Science, University of Baghdad, Baghdad, IRAQ

In this work, tin dioxide thin films were prepared by dc reactive sputtering technique. These film were deposited on glass substrates and their structural characteristics were determined by the x-ray diffraction (XRD) patterns, atomic force microscopy (AFM) and scanning electron microscopy (SEM). It is found that the XRD peaks becomes gradually sharper with increasing discharge current that indicates smaller particle size. The AFM results showed that the prepared films have granular structure and high surface area, which is very useful for gas sensing devices based on nanostructured SnO_2 thin films. As the partial amount of oxygen in the argon:oxygen mixture is increased, the surface mobility and the energy of the SnO_2 molecules increase leading to higher mean free path of the SnO_2 molecules and hence more massive grain sizes.

Keywords: Nanostructures; DC sputtering; Tin dioxide; Surface morphology
Received: 22 May 2020; **Revised:** 28 June 2020; **Accepted:** 4 July 2020

1. Introduction

Physical adsorption (physisorption) is defined as an adsorption event where no geometric change occurs to the adsorbed molecule and van der Waals forces are involved in the bonding between the surface and adsorbate [1-3]. Chemical adsorption (chemisorption) is the formation of a chemical bond between the molecule and the surface during the adsorption process and requires activation energy (e.g. ~0.5eV for chemisorption of oxygen on SnO_2) [4,5]. Chemisorption is a much stronger bond than physisorption. Two types of chemisorption occur on the surface of metal oxides: (1) molecular chemisorption, in which all the atomic bonds are preserved in the adsorbed molecule; and (2) dissociative chemisorption, where bonding within the adsorbed molecule decomposes and molecular fragments or ions are bound to oxide surface [6,7]. Molecular chemisorption is the most probable type of adsorption for molecules that possess free electrons or multiple bonds [8]. Gas molecules with single bonds tend to react via dissociative chemisorption; however; there is an activation energy associated with dissociation [9]. The type of chemisorbed oxygen on the surface of a metal oxide is dependent on the temperature of the system. The results of oxygen adsorption on SnO_2 and correlated the adsorbed oxygen species to temperature where techniques such as infrared spectroscopy and temperature programmed desorption were used [10].

2. Experimental Part

The SnO_2 films were deposited on glass substrates, which were cleaned in alcohol, distilled water and dried in air before loading into the deposition chamber. The substrates were cleaned in sputtering of Ar plasma at bias voltage of 1000 V for 5 minutes.

The thickness of SnO_2 thin films was measured by using an optical interferometer method employing He-Ne laser (0.632μm) at incident angle of 45°. This method depends on the interference of the laser beam reflected from thin film surface and the substrate, the films thickness (t) was determined using the following formula [11]

$$t = \frac{\lambda}{2} \cdot \frac{x_2}{x_1} \qquad (1)$$

where x_1 is the fringe width, x_2 is the distance between two fringes and λ is the wavelength of laser light

The prepared thin films were examined by Bruker D2 PHASER XRD technique with Cu-Kα x-ray tube (λ = 1.54056Å). The x-ray scans were recorded with the diffraction angle in the range 20-60°. The overall structure of thin films, including lattice constants, grain size identification of unknown materials, orientation of single crystals, and orientation of the crystallites were determined. The surface topography of the prepared surfaces was investigated by the atomic force microscopy (AFM) in order to confirm the formation of nanostructures within the prepared samples.

Optical measurements on the prepared thin films were performed using a UV/Visible 2601 Lambda spectrophotometer. During scanning, a blank glass slide was placed in one of the beam's direction and another glass slide with deposited film was in the other beam's direction. Thus, the absorption spectrum displayed by the UV/Visible spectrophotometer was

as a result of the films deposited on the glass slide substrates.

3. Results and Discussion

X-ray diffraction was used to study the crystal structure of SnO_2 thin films, growth on glass substrate with different; discharge current (I_d), gas pressure, and argon/oxygen mixed flow. Thin films of pure tin oxide, were investigated for their structural and surface morphological properties. Figures (1), (2) and (3) show the XRD patterns of the prepared SnO_2 thin films and table (1) shows the summary of the structural parameters obtained from the XRD patterns.

Table (1) Comparison between the experimental (Exp.) and standard (Std.) values of d_{hkl} for the peaks shown in XRD patterns for different discharge currents

I (mA)	2θ (Deg.)	FWHM (Deg)	Int. (Arb. Unit)	d_{hkl} Exp.(Å)	d_{hkl} Std.(Å)	hkl	G.S (Å)
10	-	-	-	-	-	-	-
15	-	-	-	-	-	-	-
20	26.521	0.81	280	3.358	3.3498	(110)	95
	33.214	0.79	70	2.695	2.6440	(101)	98
	51.233	1.35	40	1.778	1.7642	(211)	62
	57.751	1.37	20	1.595	1.5932	(002)	62
25	26.321	0.80	130	3.383	3.3498	(110)	97
	33.571	0.68	270	2.667	2.6440	(101)	115
	37.120	1.14	30	2.420	2.3687	(200)	69
	51.353	1.03	50	1.778	1.7642	(211)	80
	57.721	0.95	110	1.596	1.5932	(002)	90

Figure (1) shows the XRD of SnO_2 thin films were prepared at different discharge currents (10, 15, 20, and 25 mA), all SnO_2 thin films deposited on glass substrate under same conditions, mainly, the inter-electrode distance is 5 cm, the sputtering pressure is $5x10^{-2}$ mbar and sputtering time is 60 min. The diffraction pattern of the sample A and B as shown in Fig. (1) has no peaks which indicates the amorphous nature of the film. In sample C and D randomly oriented tin oxide crystalline formation starts and planes corresponding to (110), (101) and (211) appear crystal lattice planes and all other smaller peaks coincide with the tetragonal rutile structure of SnO_2. The presence of broad and weak peaks indicate that SnO_2 has very crystalline size or that SnO_2 particles are semi-crystalline in nature [12]. The unit cell consists of two metal atoms and four oxygen atoms. Each metal atom is situated a middle six oxygen atoms which approximately form the corners of a regular octahedron. Oxygen atoms are surrounded by three tin atoms which approximate the corners of an equilateral triangle. It is found that the XRD peaks becomes gradually sharper with increase in discharge current, indicating smaller particle size. Intensities corresponding to (110), (101) and (211) get enhanced with discharge current showing better crystallinity of films deposited at higher discharge current. In sample D an enhanced intensity shift toward (101) from (110) plane and a new peaks corresponding to (200) and (220) plans are seen. A disappearance of XRD peaks corresponding to some lattice planes may be caused by large number of vacant lattice sites or locale lattice disorders [13]. The calculated lattice parameters of as prepared SnO_2 thin films are given in table (2).

Table (2) Comparison of lattice constant showed in XRD for different discharge current

Discharge current (mA)	a (Å)	c (Å)	Calculated density (gm/cm^3)
10	-	-	-
15	-	-	-
20	4.7012	3.190	7.07
25	4.7362	3.192	6.96

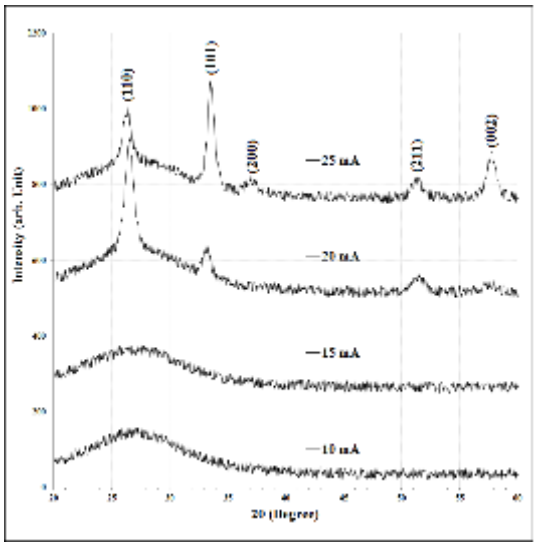

Fig. (1) XRD of sputtering SnO_2 thin films on glass substrate for different discharge currents

The XRD patterns of the deposited SnO_2 thin films using different working pressures (0.015 to 0.15 mbar), argon:oxygen mixing ratio of 1:2, sputtering time of 60 min, inter-electrode distance of 5 cm, biasing voltage of 4 kV, are shown in Fig. (2).

Reflections from the tetragonal crystallographic phase (cassiterite) of SnO_2 became more defined and progressively more intense and sharp for films with

increasing of working pressures. In all samples randomly oriented tin oxide crystalline formation starts planes corresponding to (110), (101), (211) and (002) planes of SnO_2 for 2 θ values of 26.51, 33.85, 51.69 and 57.93, respectively.

From Fig. (2) and tables (3) and (4), its clear that the films are textured and the degree of texturing depends on the value of working pressure. The change of predominant orientation of crystallites, forming gas sensitive matrix, and confirms the cassiterite structure of nanocrystalline SnO_2 [14]. The (110) is the dominant crystal structure of low-index crystal faces for this material due to its stability. This is the desired structure of SnO_2 for sensing applications since its prevalent (110) growth plane is extremely stable and can reject oxygen with little distortion [15]. The growth of this plane helps in achieving high oxygen vacancy concentrations at low temperature.

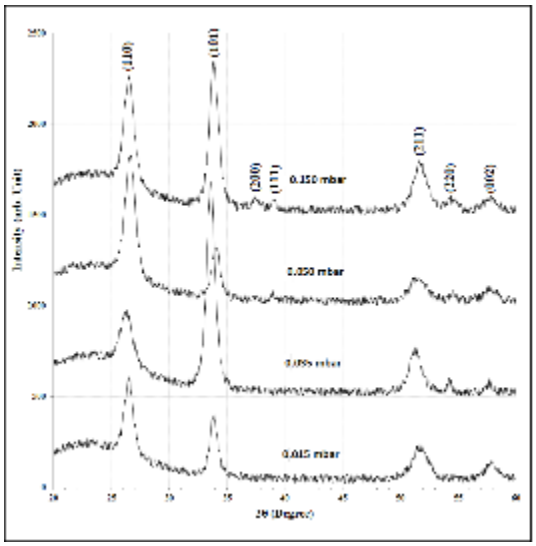

Fig. (2) XRD of sputtered SnO_2 thin films on glass substrate for different working pressure

Table (4) Comparison lattice constant showed in XRD for different discharge current

Pressure (mar)	a (Å)	c (Å)	Calc. density (gm/cm^3)
0.015	4.750	3.182	6.94
0.035	4.789	3.192	6.81
0.050	4.731	3.188	6.98
0.150	4.749	3.190	6.92

Crystal structure of films was characterized by X-ray diffraction. The XRD pattern of SnO_2 thin films deposited on glass substrate for different Ar:O_2 mixing ratios (4:1, 2:1, 1:1, 1:2 and 1:4) at optimum constant working pressure of 0.05 mbar, sputtering time of 60 min, inter-electrode distance of 5 cm, and biasing voltage of 4 kV, as shown in Fig. (3). All films are polycrystalline and the preferred orientation is in (110) direction for the films deposited using mixing ratio lower than 1 (i.e., 1:2 and 1:4). The preferred orientation was changed from (110) to (211) as the mixing ratio increased from 1 to 4.

Tables (5) and (6) demonstrate significant changes in grain size as well as in intensity of peaks. These changes are due to increase the reaction between the oxygen and the Sn target surface. On the other hand, with increased oxygen atoms, the substrate film surface would be absorbed on, to produce the (110) dominant crystal structure.

Table (6) Comparison lattice constant showed in XRD for different Ar to O2 mixed flow.

Ar/O_2	a (Å)	c (Å)	Calc. density (gm/cm^3)
1/4	4.783	3.206	6.79
1/2	4.755	3.184	6.92
1/1	4.791	3.192	6.80
2/1	4.772	3.192	6.85
4/1	4.783	3.186	6.84

The increasing of oxygen content is related to a significant increase of the density of defects. The increase in the oxygen absorption might be attributed to a change in film structure from an amorphous film containing the Sn_2O_3 phase towards a mixed phase containing SnO and SnO_2 with a large density of defects. Due to the presence of the SnO phase, the average transmission in the visible was decreased. The SnO phase is leading to the brownish color of the films which is characteristic for SnO [16]. However, the film structure is not suited to ensure a high conductivity, as confirmed by the high resistivity observed.

AFM is used to study the surface morphology with resolution of 0.1 nm. The roughness of the coated surface is an important parameter, where the surface roughness not only describes the light scattering but also gives an idea about the quality of the surface under investigation, in addition to providing some insight on the growth morphology. Two and three-dimensional AFM images of the as-deposited SnO_2 films with different discharge current, working gas pressure, and Ar/O_2 mixture flow are shown in Figs. (4), (5) and (6), respectively. The average grain size and root mean square roughness (RMS) of these films are shown in table (7). The AFM images of all samples displayed are granular structure. The granular films show higher surface area, which is conductive for film-gas interaction and results in higher gas sensitivity [17]. The gas sensitivity has a proportional relationship with film roughness [18].

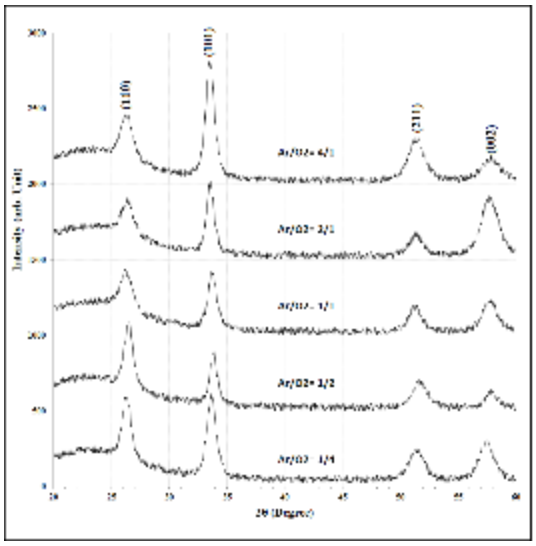

Fig. (3) XRD of sputtered SnO_2 thin films on glass substrate for different Ar to O_2 mixed flow

Figure (4) shows that the average grain size and average roughness increase from 86.14 nm and 0.0301 nm for discharge current 10 mA to 109.1 nm and 0.203 nm for discharge current 25 mA. These small grain sizes are uniformly distributed of shape and size along the film surface, with tight packed grains is observed. The increasing discharge current increased thermal energy for further increase in substrate temperature, which enhances the mobility of the atoms on the surface further to form even larger grains. As they form larger grains, the surface roughness also increases due to the formation of deeper edges. Or the roughness and average grain size was increased as the substrate temperature increase.

Figure (5) shows the decreasing in grain size from 138.29 nm at pressure 0.15 mbar to 78.73 nm at pressure 0.035 mbar and increases after that, while the roughness increases from 1.08 nm at 0.15 mbar to 1.85 nm at 0.035 mbar and decreases after that. The low dense plasma which have not enough energy to re-nucleation which leads to increase the average roughness and decreases grain size.

All images appeared in Fig. (6) show homogeneous cluster distribution with columnar structure; where the average grain size values decrease slightly with increasing of oxygen flow. Increasing oxygen flow leads to increasing in number of oxygen molecules adsorbs on the substrate surface which act as traps for atoms causing to reduce grain size for thin films by increasing in the number of nucleation centers, Also, increases roughness with increasing oxygen flow which leads to increase the vertical growth on substrate surface.

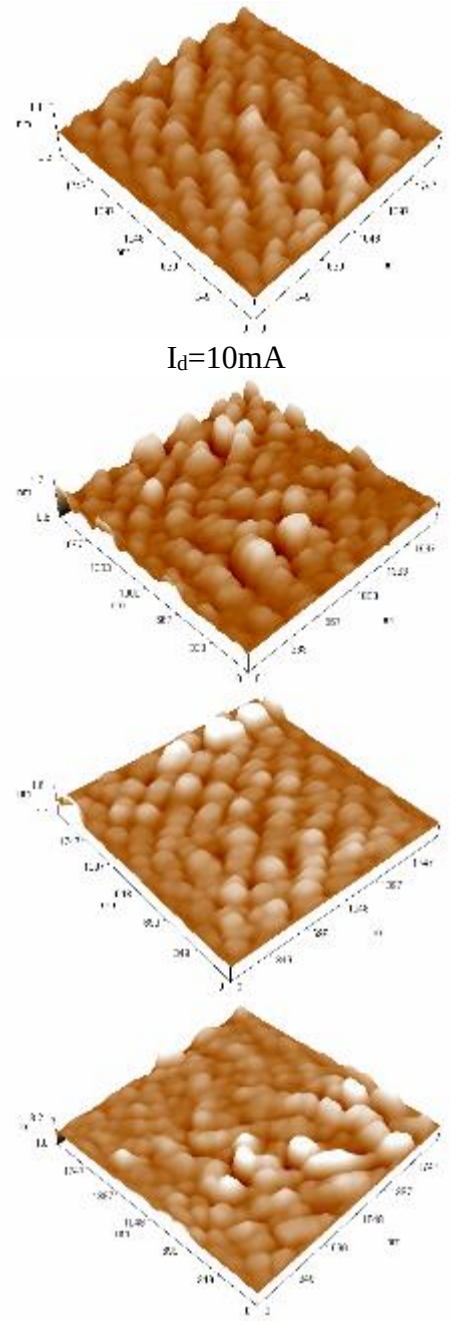

Fig. (4) The AFM images of SnO_2 thin films deposited on glass substrate for different discharge current

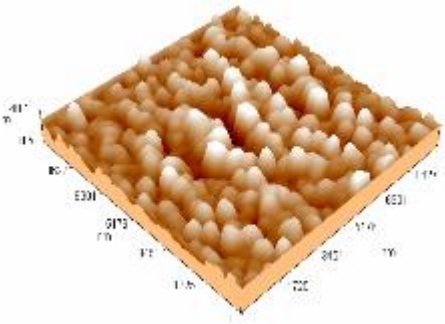

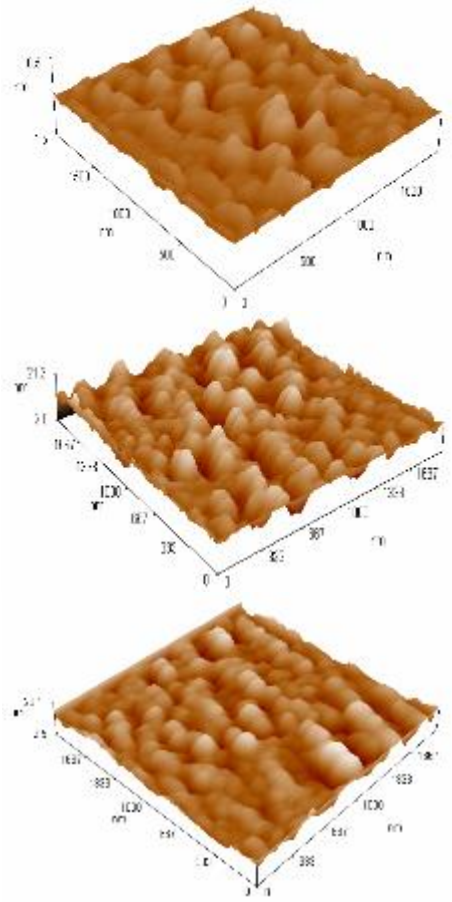

Fig. (5) The AFM images of SnO_2 thin films deposited on glass substrate for different gas pressure

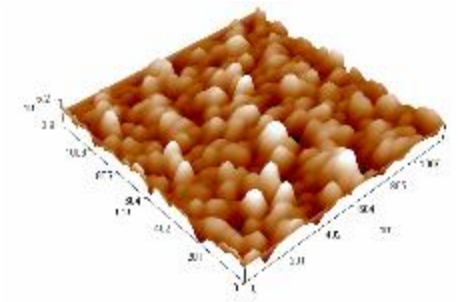

Ar/O_2=4/1

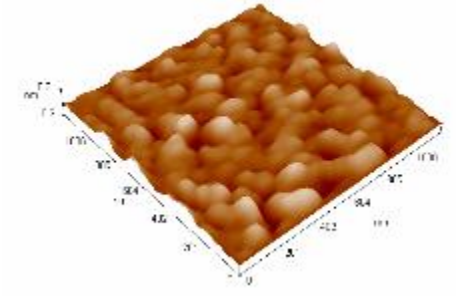

Ar/O_2=2/1

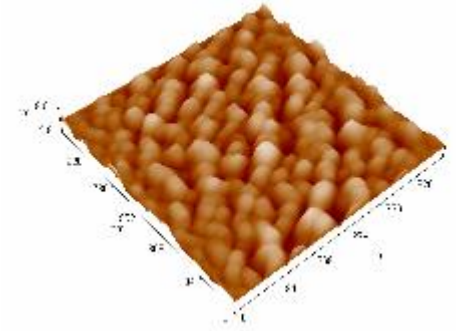

Ar/O_2=1/1

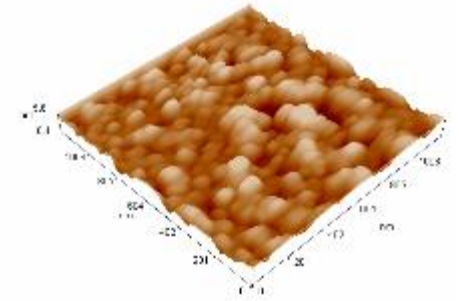

Ar/O_2=1/4

Fig. (6) The AFM images of SnO_2 thin films deposited on glass substrate for different Argon/Oxygen mixture flow

The SEM images in Fig. (7) show surface morphology of SnO_2 films grown on glass substrates under sputtering applied voltage 4kV, and 2/1 ,1/4 argon-oxygen mixture gas. It can be seen that SnO_2 films grown at 1/4 mixed gases ratio are composed of tiny grains with uniform diameters around 44.66 nm. While the grain sizes increased as increased argon-oxygen mixture gases, resulting in blend of dissimilar grain sizes. The grain sizes around 55.82nm in film grown at (2/1) mixed gas. Similar enlargement of the grain size at different argon-oxygen mixture are found in other working [19] and were explained as that when the argon-oxygen mixture increased, the surface mobility and the energy of the SnO_2 molecules increase, leading to higher mean free path of the SnO_2 molecules and hence more massive grain sizes.

Table (7) shows the surface morphology details of a film nanostructure determined by means of the AFM method with different deposition conditions. AFM characterization of the films surfaces revealed a granular, polycrystalline morphology with grain size and roughness. Also the grain size of AFM images was compared with scan electron microscope (SEM) image, which is demonstrated in Fig. (8) for two samples.

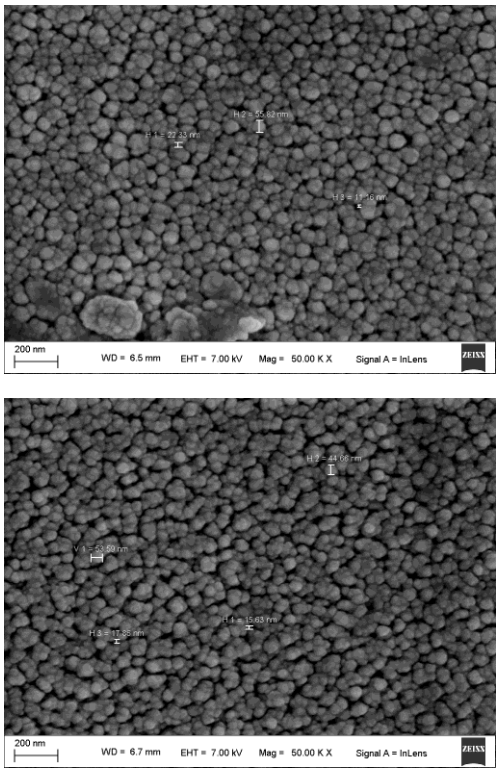

Fig. (7) The SEM images of SnO_2 thin films deposited on glass substrate at 0.05 mbar gas working pressure (a) Ar/O_2=2/1 (b) Ar/O_2=1/4

4. Conclusion

In concluding remarks, tin dioxide thin films were prepared by dc reactive sputtering technique. These film were deposited on glass substrates. It is found that the XRD peaks becomes gradually sharper with increasing discharge current that indicates smaller particle size. The AFM results showed that the prepared films have granular structure and high surface area, which is very useful for gas sensing devices based on nanostructured SnO_2 thin films. As the partial amount of oxygen in the argon:oxygen mixture is increased, the surface mobility and the energy of the SnO_2 molecules increase leading to higher mean free path of the SnO_2 molecules and hence more massive grain sizes.

References

[1] J. Hildenbrand, "Simulation and characterization of a micro machined gas sensor and preparation for model order reduction", Diploma thesis, Albert Ludwig University, Freiburg, Germany, (2003).
[2] G.E. Patil et al., "Synthesis characterization and gas sensing performance of SnO_2 thin films prepared by spray pyrolysis", Bull. Mater. Sci., 34(1) (2011) 1-9.
[3] C. Xu et al., "Grain size effects on gas sensitivity of porous SnO_2-based elements", Sensors and Actuators B, 3(2) (1991) 147-155.
[4] E.R. Beac, "Picoliter drop deposition of oxide nano-particles: a route to high performance micro sensor arrays", Ph.D. dissertation, The Ohio State University, (2009).
[5] W.S. Hu et al., "Preparation of nanocrystalline SnO_2 thin films used in chemisorption sensors by pulsed laser reactive ablation", J. Mater. Sci.: Materials in Electronics, 8 (1997) 155-158.
[6] M. Gaidi et al., "Structure and photoluminescence of ultrathin films of SnO_2 nanoparticles synthesized by means of pulsed laser deposition", J. Appl. Phys., 108(6) (2010) 063537.
[7] T.W. Kim, D.U. Lee and Y.S. Yoon, "Microstructural, electrical, and optical properties of SnO_2 nanocrystalline thin films grown on InP (100) substrates for application as gas sensor", J. Appl. Phys., 88(6) (2000) 3759-3761.
[8] J. Gong et al., "Development of Micromachined Nanocrystalline Mesoporous SnO_2 Gas Sensor for Electronic Nose", IEEE Proc., 7803 (2003) 124-128.
[9] J. Kaur, S.C. Roy and M.C. Bhatnagar, "Highly sensitive SnO_2 thin film NO_2 gas sensor operating at low temperature", Sensors and Actuators B, 123 (2007) 1090-1095.
[10] N. Barsan and U. Weimar, "Understanding the fundamental principles of metal oxide based gas sensors; the example of CO sensing with SnO_2 sensors in the presence of humidity", J. Phys.: Cond. Matter, 15 (2003) 813-839.
[11] K.L. Chopra, "Thin Film Phenomena", McGraw-Hill (NY, 1969).
[12] Z. Chen et al., "Insight on fractal assessment strategies for tin dioxide thin films", Amer. Chem. Soc., 4(2) (2010) 1202-1208.
[13] Joint Committee on Powder Diffraction Standards (JCPDS), International Center for Diffraction Data, Swarthmore, card no. 36-1451, PA, (1980).
[14] G. Korotcenkov et al., "XRD study of gas sensitive SnO_2 thin films deposition by spray pyrolsis method", Conf. Proc., vol. 1 (1999).
[15] F.R. Sensato et al., "Periodic study on the structural and electronic properties of bulk oxidized and reduced SnO_2 (110) surfaces and the interaction with O_2", Surf. Sci., 511 (2002) 408-420.
[16] J. Boltz, "Sputtered tin oxide and titanium oxide thin films as alternative transparent conductive oxides", Aachen, Techn. Hochsch., Diss., (2011) 62-65.
[17] S.C. Gadkari et al., "Solid state sensors for toxic gases", Tech. Phys. Proto. Eng. Div. Bhabha Atomic Res. Centre, Issue. 49 (2005).
[18] N.G. Deshpandea et al., "Studies on tin oxide-intercalated polyaniline nanocomposite for ammonia gas sensing applications", Sensors and Actuators B, 138 (2009) 76-84.
[19] Z.H.W. "Preparation and piezoresistive characteristics of polycrystalline SnO_2 films", IEEE Xplore, 15 (1995) 154-157.

Table (3) Comparison between the Exp. and Std. value of d_{hkl} for the peaks showed in XRD for different gas pressure

P (mbar)	2θ (Deg.)	FWHM (Deg)	Int. (Arb. Unit)	d_{hkl} Exp. (Å)	d_{hkl} Std. (Å)	hkl	G.S (Å)
0.015	26.51	0.89	412	3.359	3.3498	(110)	86
	33.85	0.75	335	2.646	2.6440	(101)	103
	51.69	1.56	175	1.767	1.7642	(211)	53
	57.93	1.41	83	1.591	1.5932	(002)	61
0.035	26.30	1.27	285	3.386	3.3498	(110)	60
	33.61	0.85	1129	2.664	2.6440	(101)	92
	51.29	1.29	228	1.780	1.7642	(211)	64
	54.25	0.32	62	1.689	1.6749	(220)	314
	57.70	0.51	53	1.596	1.5932	(002)	167
0.050	26.63	1.024	659	3.345	3.3498	(110)	75
	34.03	0.85	265	2.632	2.6440	(101)	92
	38.98	0.22	44	2.308	2.3087	(111)	356
	51.53	1.61	134	1.772	1.7642	(211)	53
	54.50	0.61	38	1.682	1.6749	(220)	145
	57.81	1.20	68	1.594	1.5932	(002)	71
0.150	26.52	1.00	594	3.358	3.3498	(110)	76
	33.87	0.89	798	2.644	2.6440	(101)	87
	37.52	0.78	53	2.395	2.3687	(200)	101
	38.98	0.61	39	2.309	2.3087	(111)	141
	51.71	1.30	256	1.766	1.7642	(211)	62
	54.43	1.18	52	1.684	1.6749	(220)	71
	57.76	1.22	63	1.595	1.5932	(002)	69

Table (5) Comparison between the Exp. and Std. value of d_{hkl} for the peaks showed in XRD for different Ar to O_2 mixed flow

Ar/O_2	2θ (Deg.)	FWHM (Deg)	Int. (Arb. unit)	d_{hkl} Exp. (Å)	d_{hkl} Std.(Å)	hkl	G.S. (Å)
1/4	26.33	0.88	407	3.382	3.3498	(110)	87
	33.67	0.95	531	2.660	2.6440	(101)	82
	51.40	1.55	191	1.776	1.7642	(211)	54
	57.45	1.50	246	1.603	1.5932	(002)	57
1/2	26.49	0.87	417	3.362	3.3498	(110)	88
	33.85	0.74	330	2.646	2.6440	(101)	106
	51.72	1.36	166	1.766	1.7642	(211)	61
	57.86	1.18	96	1.592	1.5932	(002)	72
1/1	26.28	1.27	246	3.388	3.3498	(110)	61
	33.73	0.88	362	2.655	2.6440	(101)	88
	51.28	1.38	154	1.780	1.7642	(211)	60
	57.70	1.50	205	1.596	1.5932	(002)	57
2/1	26.39	1.21	222	3.374	3.3498	(110)	63
	33.57	0.77	465	2.667	2.6440	(101)	102
	51.35	1.55	134	1.778	1.7642	(211)	54
	57.72	1.78	377	1.596	1.5932	(002)	48
4/1	26.33	1.23	285	3.382	3.3498	(110)	62
	33.55	0.88	770	2.669	2.6440	(101)	88
	51.38	1.57	276	1.777	1.7642	(211)	53
	57.83	1.90	140	1.593	1.5932	(002)	45

Table (7) The AFM and SEM data images of SnO_2 thin films deposited on glass substrate for different condition

Discharge current (mA)	Gas pressure (mbar)	Argon/Oxygen mixture flow	Average Roughness (nm)	Average Grain Size (nm)
10	0.05	1/2	0.0301	86.14
15	0.05	1/2	0.103	79.93
20	0.05	1/2	0.0455	93.85
25	0.05	1/2	0.203	109.1
Biasing voltage (kV)	Gas pressure (mbar)	Argon/Oxygen mixture flow	Average Roughness (nm)	Average Grain Size (nm)
4	0.15	1/2	1.08	138.29
4	0.05	1/2	0.353	98.66
4	0.035	1/2	1.85	78.73
4	0.015	1/2	1.58	97.19
Biasing voltage (kV)	Gas pressure (mbar)	Argon/Oxygen mixture flow	Average Roughness (nm)	AFM Average Grain Size (nm)
4	0.05	4/1	0.613	72.22
4	0.05	2/1	0.526	71.05
4	0.05	1/1	1.58	56.91
4	0.05	1/4	0.604	60.52